Engineering Journal issn: 0125-8281

Article

Design of 2D-Lattice Plates by Weight Efficiency

Pana Suttakul[1,a], **Ekachai Chaichanasiri**[2,b], **and Pruettha Nanakorn**[1,c,*]

1 School of Civil Engineering and Technology, Sirindhorn International Institute of Technology, Thammasat University, Pathumthani, Thailand
2 Department of Mechanical Engineering, Faculty of Engineering, Mahidol University, Nakhon Pathom, Thailand
E-mail: [a]pana.s@cmu.ac.th, [b]ekachai.cha@mahidol.ac.th, [c,*]nanakorn@siit.tu.ac.th (Corresponding author)

Abstract. In this study, a method to design 2D-lattice plates, based on their weight efficiency, is proposed. The 2D-lattice plates considered in this study are made up of Euler-Bernoulli beams and can be modeled as homogeneous orthotropic Kirchhoff plates, derived by the strain-energy-based homogenization method. The weight efficiency of 2D-lattice plates is evaluated using relationships between their effective rigidities and area weight densities. The proposed design method is developed with these relationships. The closed-form effective rigidities of 2D-lattice plates, derived by the strain-energy-based homogenization method, are utilized as convenient design formulas for the proposed design method. A generic symbolic finite element program, written in MATLAB, is used to determine the closed-form solutions of effective properties that include the effective elastic constants, the effective rigidities, and the relationships between the effective rigidities and the area weight densities of 2D-lattice plates. Example design graphs, created by the obtained closed-form solutions, for 2D-lattice plates with different unit cells are presented and discussed. In addition, the usefulness of the obtained weight efficiency is also demonstrated via analysis of 2D-lattice plates with different unit-cell patterns.

Keywords: 2D-lattice plate, weight efficiency, effective rigidity, homogenization, closed-form solution.

ENGINEERING JOURNAL Volume 25 Issue 11
Received 7 April 2021
Accepted 21 November 2021
Published 30 November 2021
Online at https://engj.org/
DOI:10.4186/ej.2021.25.11.13

DOI:10.4186/ej.2021.25.11.13

1. Introduction

Two-dimensional lattices are periodic structures that are used in a wide range of applications, such as structural panels and floors, aircraft structural parts [1-4], heat exchangers [5], and biomaterials [6,7]. Structures of this type are attractive because they are lightweight when compared to their full-solid counterparts and their patterns can be designed to yield required overall properties [8-11]. In addition, they can usually be mass-produced. Two-dimensional lattices can be considered as structures that are obtained hypothetically by removing some materials from their original full-solid structures. Naturally, 2D lattices are lighter than their original full structures while the stiffness is also reduced. When the stiffness of a 2D lattice is the main design target, a method to minimize the stiffness reduction with respect to the weight reduction, due to the hypothetical material removal from an original full-solid counterpart, is desirable. The relationship between stiffness and weight can be used to determine the weight efficiency of 2D lattices having different periodic patterns. Two-dimensional lattices can be used as plane or plate structures. When the size of a 2D-lattice plate is significantly larger than the sizes of its unit cells, the lattice can be accurately represented by an equivalent full-solid plane or plate structure having an equivalent homogeneous solid. By using the properties of the equivalent homogeneous solid, modeling of the equivalent structure can be done more easily than the modeling of the original lattice.

The effective properties of the equivalent homogeneous solid of a 2D lattice can be determined by homogenization methods [10,12-27]. A homogenization method can be used to theoretically replace a material that has uniformly distributed inhomogeneities on a small scale with an equivalent homogeneous material on a large scale. This allows materials with uniformly distributed small inhomogeneities to be conveniently considered as homogeneous materials. One of the most widely used homogenization methods is the strain-energy-based homogenization method [15,28-30]. In this method, the strain energy in an equivalent homogeneous material, under uniform far-field boundary conditions, is considered to be the same as the strain energy in its original inhomogeneous material, under the same boundary conditions [15]. The relationship between the average stresses and average strains that occur in the inhomogeneous material under these boundary conditions is considered as the effective material law of the material.

Two-dimensional-lattice plates are generally frame-like and can therefore be modeled as frame structures, with their struts considered as beams. The effective material law of a 2D-lattice plate can be determined by the strain-energy-based homogenization method through frame analysis of a selected unit cell of the plate. Since unit cells of practical 2D-lattice plates do not usually have many strut members, the analysis of unit cells may be performed analytically, instead of numerically, to obtain the closed-form effective elastic constants of these plates. Closed-form solutions, if obtainable, are preferred since they can be conveniently used as engineering formulas. Several modern mathematical software packages can facilitate these analytical derivations. Closed-form effective elastic constants of plane-stress lattices with various unit-cell patterns have been determined by Masters and Evans [31], Gibson and Ashby [17], Wang and McDowell [18], Vigliotti and Pasini [21], and Sam et al. [27]. Some of these derivations have been done manually while some have been carried out with the help of symbolic mathematical software packages. In the work by Sam et al. [27], a generic symbolic finite element program, written in MATLAB, is used to analytically derive the effective elastic constants of frame-like periodic solids having various unit-cell patterns. In their study, the strain-energy-based homogenization method is used, and 2D frame-like periodic solids under the plane-stress condition and 3D frame-like periodic solids are considered. Exact parametric forms of the effective material constants for 2D-lattice plates are analytically derived by Suttakul et al. [32]. The forms contain some dimensionless factors. When these dimensionless factors are constants, their values can be determined by exact curve fitting, and the closed forms of the effective material constants can be obtained. In contrast, when the dimensionless factors are not constants, it is not possible to obtain the closed-form solutions by their methodology.

In this paper, a method to design 2D-lattice plates with different unit-cell topologies, based on their weight efficiency with respect to their effective rigidities, is proposed. The proposed design method uses the relationships between the effective rigidities and the area weight densities of 2D-lattice plates to determine their weight efficiency, and design solutions are determined from these relationships. In practice, design methods are mostly given with formulas. It is therefore desirable that the design method proposed in this study can also be given with formulas. To demonstrate this possibility, the symbolic finite element program in the work by Sam et al. [27] is used to determine the closed-form effective rigidities of 2D-lattice plates having some common unit-cell topologies. These unit cells are square, body-centered square, diamond-square, triangular, hexagonal, diamond, and kagome unit cells. It is assumed that the struts of these unit cells can be modeled accurately as Euler-Bernoulli beams. As a result, it is also assumed that the equivalent homogenous plate of a 2D-lattice plate behaves as a homogeneous orthotropic Kirchhoff plate. The obtained closed-form effective rigidities can then be used to provide essential design formulas. The work by Sam et al. [27] provides the closed-form effective in-plane rigidities of 2D lattices with several common unit-cell patterns, but not the closed-form effective out-of-plane rigidities. As a result, the closed-form effective out-of-plane rigidities obtained in this study extend the work by Sam et al. [27]. In addition, they can also be used to verify the solutions obtained by exact curve fitting in the work by Suttakul et al. [32].

In the analytical derivations in this study, the symbolic finite element program is used to analytically compute the strain energy of unit cells under various curvature modes. These closed-form expressions of the strain energy are subsequently used to analytically compute the closed-form effective elastic constants and effective rigidities of the resulting 2D-lattice plates. The closed-form relationships between the effective rigidities and the area weight densities of these plates are also determined. These closed-form relationships allow the weight efficiency, with respect to the effective rigidities, of the resulting 2D-lattice plates to be determined. Examples of design graphs for 2D-lattice plates with different unit cells, constructed from the closed-form solutions in this study, are shown. Finally, the usefulness of the obtained weight efficiency is also demonstrated through analysis of 2D-lattice plates with some different unit-cell patterns.

The 2D-lattice plates considered in this study are frames consisting of Euler-Bernoulli beams and can be modeled as homogeneous orthotropic Kirchhoff plates. This scope of consideration allows convenient closed-form design formulas to be derived. However, the scope also limits the applicability of these design formulas only to 2D-lattice plates that can be modeled accurately as frames of Euler-Bernoulli beams. For 2D-lattice plates consisting of thick beams that can be modeled accurately as frames of Timoshenko beams, a different set of closed-form design formulas can be derived. There are lattice structures that consist of only Euler-Bernoulli or Timoshenko beams, but their unit-cell topologies contain joints, each of which connects a significant number of struts. Consequently, these joints contain large volumes of material. As a result, modeling these structures as frames may yield inaccurate results since, in normal frame analysis, joints are modeled as points, and their geometrical details are ignored. Frame analysis cannot be used for lattice structures that are made up of 3D solid continua. For these structures, 3D solid modeling is necessary [33-35]. Unfortunately, when 3D solid modeling is required and used, it is virtually impossible to obtain closed-form design formulas.

The concept of designing unit cells of cellular solids for required macroscopic properties has been studied by many researchers. In a broader scope, the components of a cellular solid at different scales can be considered together and designed. This broader concept is usually called the multiscale design concept. Since some design tasks for a cellular solid can be directly performed solely on its unit cell, it is possible to employ an optimization method to facilitate these design tasks. For example, Gu et al. [5] proposed an optimization technique for designing 2D cellular metals for combined heat dissipation and structural load capacity by considering cell morphologies and cell arrangements. Design strategies dealing with multiscale optimal design of sandwich panels with cellular cores can be found in the works by Catapano and Montemurro [9], Catapano and Montemurro [36], and Montemurro et al. [37]. Similar design strategies for shape optimization of cellular structures have also been proposed by Bertolino et al. [8] and Montemurro et al. [38]. Theerakittayakorn et al. [10] presented a simple strategy for designing frame-like periodic structures for isotropic symmetry by appropriate sizing of their unit-cell struts. Approaches for designing 2D auxetic periodic structures by modifying their re-entrant honeycomb unit cells have been given in the works by Lu et al. [11] and Baran and Öztürk [39].

This paper is organized into seven sections. Section 2 presents the definitions of the effective bending rigidities and torsional rigidity of a thin periodic plate. These rigidities are then used to construct parameters for assessing the weight efficiency of 2D-lattice plates in the same section. Section 3 discusses how the effective properties of 2D-lattice plates can be determined by the strain-energy-based homogenization method. Section 4 briefly mentions the symbolic finite element program used in this study. Section 5 presents the closed-form effective elastic constants and rigidities of 2D-lattice plates having the unit-cell topologies considered in this study. After that, the design method for weight efficiency is proposed in Section 6, in which some example design graphs are also given. The paper is concluded in Section 7.

2. Weight Efficiency of 2D-Lattice Plates

This study considers 2D-lattice plates that consist of Euler-Bernoulli beams and can be modeled as homogeneous orthotropic Kirchhoff plates [32]. To describe an orthotropic Kirchhoff plate, the conventions in Fig. 1 are used. In the figure, x_1 and x_2 are the orthotropic axes of the plate. In addition, M_{11}, M_{22}, M_{12}, and M_{21} are the bending moments while Q_1 and Q_2 are the shear forces. These internal forces are quantities per unit length. Moreover, h in the figure is the plate thickness.

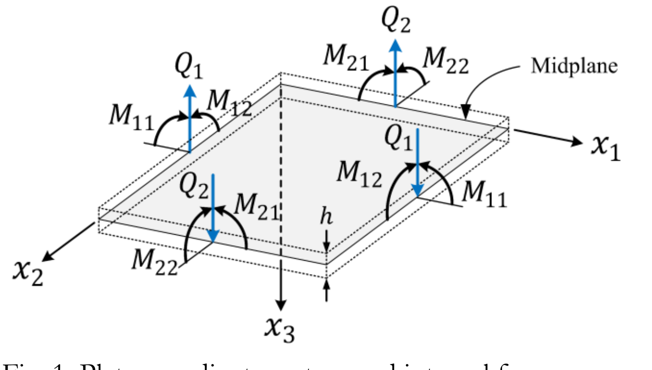

Fig. 1. Plate coordinate system and internal forces.

Lattice patterns are used in plates to reduce the weights of the plates. When the plate rigidities are among the main design targets, the design efficiency can be evaluated using the ratios of the plate rigidities to the area weight densities. The area weight density of a plate is defined simply as the weight of the plate per its midplane area. A plate is considered to have high weight efficiency if it has high rigidities per area weight density. In this study, the bending and torsional rigidities of orthotropic

DOI:10.4186/ej.2021.25.11.13

Kirchhoff plates defined in the work by Suttakul et al. [32] are adopted, i.e.

$$R_{b1} = \frac{E_1 h^3}{12} \quad R_{b2} = \frac{E_2 h^3}{12} \quad R_{t12} = \frac{G_{12} h^3}{12} . \tag{1}$$

Here, R_{b1} is the bending stiffness of an orthotropic plate measured when only M_{11} is applied to the plate while R_{b2} is the bending stiffness measured when only M_{22} is applied. In addition, R_{t12} is the torsional stiffness measured when only M_{12} is applied to the plate. In these definitions, E_1 and E_2 are Young's moduli and G_{12} is the shear modulus of the orthotropic material of which the plate is made. Note that, ν_{12} and ν_{21}, which will appear later in this paper, denote Poisson's ratios of an orthotropic material.

A thin periodic plate consisting of a sufficiently substantial number of unit cells can be modeled accurately as a homogeneous thin plate with effective properties. The effective bending rigidities R^*_{bi} and torsional rigidity R^*_{t12} of a thin periodic plate can be defined straightforwardly using Eq. (1) as [32]

$$R^*_{b1} = \frac{E^*_1 h^3}{12} \quad R^*_{b2} = \frac{E^*_2 h^3}{12} \quad R^*_{t12} = \frac{G^*_{12} h^3}{12} \tag{2}$$

where E^*_i and G^*_{12} are, respectively, the effective Young's moduli and effective shear modulus of the periodic plate. In addition, h is the apparent thickness of the plate.

If the plate consists only of one homogeneous base material with voids, the area weight density of the plate is given by

$$\rho^*_A = \frac{V_s \rho}{V/h} = V_f \rho h \tag{3}$$

where V and V_s represent, respectively, the volumes of the plate and the base material. In addition, ρ is the weight density of the base material and V_f is its volume fraction.

By using Eqs. (2) and (3), the effective rigidities per area weight density are obtained as

$$\frac{R^*_{bi}}{\rho^*_A} = \frac{E^*_i h^3}{12\rho^*_A} = \frac{E^*_i h^2}{12 V_f \rho} \qquad \frac{R^*_{t12}}{\rho^*_A} = \frac{G^*_{12} h^2}{12 V_f \rho} . \tag{4}$$

The above effective rigidities per area weight density are also referred to as the specific effective rigidities. Note that, in the work by Suttakul et al. [32], the specific effective rigidities are defined as the effective rigidities per weight density. Using the area weight density, instead of the overall weight density, allows the weight efficiency of 2D-lattice plates having different thicknesses, in addition to different unit-cell patterns, to be compared.

The specific effective rigidities can be further normalized by the specific rigidities of a full-solid plate having the same thickness to give

$$\begin{aligned} \hat{Z}^*_{bi} &= \frac{\left(\frac{E^*_i h^2}{12 V_f \rho}\right)}{\left(\frac{E h^2}{12\rho}\right)} = \frac{1}{V_f}\frac{E^*_i}{E} \\ \hat{Z}^*_{t12} &= \left(\frac{G^*_{12} h^2}{12 V_f \rho}\right) \Big/ \left(\frac{G h^2}{12\rho}\right) = \frac{1}{V_f}\frac{G^*_{12}}{G} \\ &= \frac{1}{V_f}\frac{G^*_{12}}{E/[2(1+\nu)]} . \end{aligned} \tag{5}$$

Here, E and G are, respectively, Young's modulus and the shear modulus of the base material. In addition, ν is Poisson's ratio. The terms, $\hat{Z}^*_{bi}$ and $\hat{Z}^*_{t12}$, are called, respectively, the normalized specific effective bending and torsional rigidities. These normalized specific effective rigidities are found to be the same as those presented by Suttakul et al. [32]. However, Suttakul et al. [32] defined the normalized specific effective rigidities based on the weight density, not the area weight density.

The effective rigidities per area weight density in Eq. (4) can be used to compare the weight efficiency of periodic Kirchhoff plates that have different unit-cell patterns and different thicknesses. The normalized specific effective rigidities in Eq. (5) can be used to assess specifically the efficiency of unit-cell patterns in terms of the weight efficiency of their resulting plates.

3. Effective Properties of 2D-Lattice Plates

When inhomogeneities of an inhomogeneous plate are uniformly distributed and considerably smaller than the plate's size, the plate can be considered as a homogeneous plate. In this case, the relationships between the average moments and average curvatures of the plate under uniform far-field boundary conditions can be used to define the plate's effective rigidities [32]. To apply uniform far-field boundary conditions, the plate has to be theoretically extended to become an infinite plate. If the inhomogeneities of the plate are periodically distributed, under uniform far-field boundary conditions, the moments and curvatures in the plate are periodic, except in the negligible regions near the far-field boundary. As a result, the average moments and average curvatures can be computed from the periodic moments and curvatures. This allows periodic far-field boundary conditions to be conveniently used instead of uniform far-field boundary conditions. Subsequently, since periodic far-field boundary conditions result in periodic moments and curvatures, a smaller domain, within the infinite plate, under appropriate periodic boundary conditions can be considered instead of the infinite plate. This smaller domain can even be one unit cell. Since the moments and curvatures are periodic, the averages can also be conveniently obtained from one unit cell. Here, some equations for the determination of the effective rigidities of thin periodic plates are briefly shown. Detailed information can be found in the work by Suttakul et al. [32].

Consider a thin periodic plate that is made of a substantial number of unit cells. The plate has a plane of reflection symmetry, which is referred to as a midplane A. The $x_1 - x_2 - x_3$ coordinate system in Fig. 1, whose origin is on the midplane A, is used as the reference frame. Although the real thickness of the plate may not be constant, it is considered as having an apparent thickness of h. The periodicity of the plate material is only in the $x_1 - x_2$ plane. Again, x_1 and x_2 are the orthotropic axes of the plate. Periodic kinematic boundary conditions are applied to the plate to create the following deflection w, i.e.,

$$\begin{aligned} w(x_1,x_2) &= w^o(x_1,x_2) + w^p(x_1,x_2) \\ &= \left[\frac{\kappa_{11}^o}{2}x_1^2 + \frac{\kappa_{22}^o}{2}x_2^2 + \kappa_{12}^o x_1 x_2\right] + w^p(x_1,x_2) \end{aligned} \tag{6}$$

where κ_{ij}^o is a constant symmetric tensor. In addition, w^p is a periodic function of x_1 and x_2. In the above equation, w^o represents the deflection of a homogeneous plate subjected to uniform kinematic boundary conditions that yield a constant curvature of κ_{ij}^o. Voids can be considered as the limit cases of infinitely soft inclusions [15]. Thus, the deflection w in the above equation is mathematically extended everywhere in the midplane of the plate, including the inside of any voids. The rotation $\theta_i = w_{,i}$ and the curvature $\kappa_{ij} = w_{,ij}$ of the periodic plate can be obtained as

$$\theta_i = w_{,i} = w_{,i}^o + w_{,i}^p = \theta_i^o + \theta_i^p \tag{7}$$

$$\kappa_{ij} = w_{,ij} = w_{,ij}^o + w_{,ij}^p = \kappa_{ij}^o + w_{,ij}^p = \kappa_{ij}^o + \kappa_{ij}^p. \tag{8}$$

Note that κ_{ij}^p and κ_{ij} are periodic since w^p is periodic and κ_{ij}^o is constant.

It can be proven that the average of κ_{ij} over A, denoted here by $\langle\kappa_{ij}\rangle$, is equal to κ_{ij}^o [32], i.e.

$$\langle\kappa_{ij}\rangle = \frac{1}{A}\int_A \kappa_{ij}\,dA = \kappa_{ij}^o. \tag{9}$$

The effective rigidity tensor D_{ijkl}^* of the periodic plate is defined as

$$\begin{aligned} \langle M_{ij}\rangle = M_{ij}^o &= \frac{1}{A}\int_A M_{ij}\,dA = -D_{ijkl}^*\langle\kappa_{kl}\rangle \\ &= -D_{ijkl}^*\kappa_{kl}^o. \end{aligned} \tag{10}$$

where $\langle M_{ij}\rangle = M_{ij}^o$ is the average of M_{ij} over A.

The average strain energy of the plate $\bar{U}$ over A is given by [32]

$$\begin{aligned} \bar{U} &= -\frac{1}{2A}\int_A M_{ij}\kappa_{ij}\,dA = -\frac{1}{2}\langle M_{ij}\rangle\langle\kappa_{ij}\rangle \\ &= \frac{1}{2}D_{ijkl}^*\kappa_{kl}^o\kappa_{ij}^o. \end{aligned} \tag{11}$$

Subsequently, the strain energy of the unit cell U_C is given by

$$U_C = \bar{U}A_C = \frac{1}{2}D_{ijkl}^*\kappa_{kl}^o\kappa_{ij}^o A_C \tag{12}$$

where A_C denotes the midplane area of the unit cell. Equation (12) is used to determine D_{ijkl}^*. In the determination of D_{ijkl}^*, different modes of κ_{ij}^o are applied to the unit cell and the strain energy values of the unit cell are determined from structural analysis. These modes of κ_{ij}^o are created via periodic boundary conditions determined from Eq. (6). The corresponding values of U_C and κ_{ij}^o are then used in Eq. (12) to compute D_{ijkl}^*.

For mathematical convenience, Eq. (10) is written in matrix form as

$$\begin{aligned} \boldsymbol{M}^o = \begin{Bmatrix} M_{11}^o \\ M_{22}^o \\ M_{12}^o \end{Bmatrix} &= -\begin{bmatrix} D_{11}^* & D_{12}^* & 0 \\ & D_{22}^* & 0 \\ Sym & & D_{33}^* \end{bmatrix}\begin{Bmatrix} \kappa_{11}^o \\ \kappa_{22}^o \\ 2\kappa_{12}^o \end{Bmatrix} \\ &= -\boldsymbol{D}^*\boldsymbol{\kappa}^o. \end{aligned} \tag{13}$$

In Eq. (13), there are four independent effective constants, i.e. D_{11}^*, D_{22}^*, D_{33}^*, and D_{12}^*, which can be determined from Eq. (12) by prescribing four different modes of κ_{ij}^o to the considered unit cell. A detailed methodology for obtaining D_{ij}^* can be found in the work by Suttakul et al. [32].

The effective elastic constants can then be obtained in terms of D_{ij}^* as [32]

$$\begin{aligned} E_1^* &= \frac{12D_{11}^*}{h^3}\left[1 - \frac{D_{12}^*}{D_{11}^*D_{22}^*}\right] \quad E_2^* = \frac{D_{22}^*}{D_{11}^*}E_1^* \\ \nu_{12}^* &= \frac{D_{12}^*}{D_{22}^*} \quad \nu_{21}^* = \frac{D_{12}^*}{D_{11}^*} \quad G_{12}^* = \frac{12D_{33}^*}{h^3}. \end{aligned} \tag{14}$$

Here, ν_{12}^* and ν_{21}^* denote the effective Poisson's ratios. Note that $\nu_{12}^*E_2^*$ is equal to $\nu_{21}^*E_1^*$. The effective elastic moduli E_i^* and G_{12}^* in Eq. (14) are used to compute all the terms defined in Eqs. (2), (4), and (5).

4. Symbolic Finite Element Program

The relationships between the effective rigidities and the area weight density of a 2D-lattice plate describe the weight efficiency of the plate. These relationships can be used to determine efficient designs of 2D-lattice plates. It is preferable that these relationships are given in closed forms as they can be used as design formulas. As the 2D-lattice plates considered in this study consist only of Euler-Bernoulli beams, it is possible to use symbolic computation to derive these relationships. In this study, a symbolic finite element program developed in MATLAB by Sam et al. [27] is used to determine the required closed-form effective properties of 2D-lattice plates. In the development of the program by Sam et al. [27], the object-oriented programming paradigm is used to increase the program's maintainability, extensibility, and reusability. In the work by Sam et al. [27], the program is used to determine the closed-form effective elastic constants of several 2D and 3D frame-like periodic solids that are made of various unit-cell patterns.

As mentioned above, the four independent effective constants, i.e. D_{11}^*, D_{22}^*, D_{33}^*, and D_{12}^* in Eq. (13), can be obtained from Eq. (12) by prescribing four different modes of κ_{ij}^o to the considered unit cell. By using the symbolic finite element program, the analytical expressions of strain energy under the four different curvature modes are symbolically determined first. After that, Eq. (12) is used to symbolically determine D_{11}^*, D_{22}^*, D_{33}^*, and D_{12}^*. After D_{11}^*, D_{22}^*, D_{33}^*, and D_{12}^* are known, the effective elastic constants in Eq. (14) can also be symbolically computed. Subsequently, the closed forms of E_i^* and G_{12}^* are used to compute the closed-form effective rigidities in Eq. (2), the effective rigidities per area weight density in Eq. (4), and the normalized specific effective rigidities in Eq. (5).

5. Effective Elastic Constants and Rigidities

In this Section, the closed-form effective elastic constants and rigidities of 2D-lattice plates having the considered unit-cell topologies are presented. The unit cells considered in this study are shown in Fig. 2. They are square, body-centered square, diamond-square, triangular, hexagonal, diamond, and kagome unit cells. The boundary edges of the unit cells are illustrated as dashed lines. The directions of the x_1 and x_2 coordinates for all unit cells in Fig. 2 are shown in the first unit cell. In the figure, L represents the selected characteristic length of each unit cell. Note that proper consideration must be given to edge struts that are shared by adjacent unit cells. As an example, consider a 2D-lattice plate made of triangular unit cells in Fig. 3. The selected unit cell is shown in Fig. 3(b). The moment of inertia and the effective polar moment of inertia of the struts are denoted, respectively, by I and J_{ef}. In finite element analysis, this unit cell is modeled as a frame structure consisting of Euler-Bernoulli beams. The bending and torsional rigidities of each horizontal edge strut of the triangular unit cell in Fig. 3(b) are only half of those of the original strut. This is because each horizontal edge strut is shared by two adjacent unit cells.

Table 1 shows the closed-form effective elastic constants of the 2D-lattice plates determined by the symbolic finite element program. It can be seen that, in most cases, the effective elastic constants are functions of the elastic properties of the base material and the sectional properties of the struts. In addition, E_i^* and G_{12}^* are found to be functions of the plate thickness h and the unit-cell characteristic length L. The closed forms in Table 1 are written in such a way that the contributions from the bending and torsional rigidities of the struts are distinguishable from each other. Regarding the elastic properties of the base material, if the relationship between E and G, i.e. $G = E/[2(1+\nu)]$, is used in the solutions in Table 1, then E_i^* can be rewritten as functions of E and ν, and these functions vary linearly with E. Similarly, G_{12}^* can be rewritten as functions of G and ν, and these functions vary linearly with G. Moreover, ν_{ij}^* can be rewritten in terms of ν alone. The exception is only for the case of the square unit cell, in which E_i^* can be written as a linear function of E alone, and G_{12}^* can be written as a linear function of G alone. For the square unit cell, ν_{12}^* and ν_{21}^* are equal to zero.

Except for the effective shear modulus G_{12}^* of 2D-lattice plates with hexagonal unit cells, the solutions in Table 1 agree exactly with the solutions by Suttakul et al. [32]. In the work by Suttakul et al. [32], a methodology is proposed to obtain the closed-form effective elastic constants of 2D-lattice plates from the exact parametric forms containing some dimensionless factors by exact curve fitting. Their methodology relies on a condition that, if all dimensionless factors in the exact parametric forms of the effective elastic constants are constant, these factors can be determined by exact curve fitting. The methodology also includes a validation procedure to numerically verify whether each closed-form effective elastic constant obtained is valid or not. In their work, the methodology is successfully used to determine the closed-form effective elastic constants of 2D-lattice plates having the unit cells considered in this study, except for the effective shear modulus G_{12}^* of 2D-lattice plates with hexagonal unit cells. This implies that some dimensionless factors in the effective shear modulus G_{12}^* of 2D-lattice plates with hexagonal unit cells are not constant. In order to check the validity of the closed-form effective shear modulus G_{12}^* of 2D-lattice plates with hexagonal unit cells obtained in this study, the same validation procedure as used in the work by Suttakul et al. [32] is performed. By considering several different hexagonal unit cells, several values of G_{12}^*, obtained numerically from the closed form of G_{12}^* in Table 1, are compared with those obtained numerically from Eqs. (12) and (14) using the values of strain energy from finite element analysis of these unit cells under the four curvature modes. Good agreement between the two sets of results is observed. Therefore, it can be concluded that all closed-form elastic constants in Table 1 are accurate.

Note that periodic boundary conditions used to create different curvature modes are in fact constraint equations that prescribe relative values between different degrees of freedom. In commercial finite element software, constraint equations of this kind are called multi-point or multi-freedom constraints. They can be incorporated into finite element analysis using the method of Lagrange multipliers. More details about periodic boundary conditions can be found in the work by Suttakul et al. [32].

DOI:10.4186/ej. 2021.25.11.13

As in symbolic finite element analysis, in numerical finite element analysis used for validating the obtained closed-form results, two-noded Euler-Bernoulli beam elements are used. This type of element employs linear and cubic interpolations for axial and transverse displacements, respectively. If an Euler-Bernoulli beam element is only subjected to end forces, these interpolations yield exact solutions of the Euler-Bernoulli beam theory. Since each unit-cell strut in this study is only subjected to end forces, using one two-noded Euler-Bernoulli beam element per strut is sufficient to obtain exact solutions of the Euler-Bernoulli beam theory. There is no need to use a mesh that is finer than that.

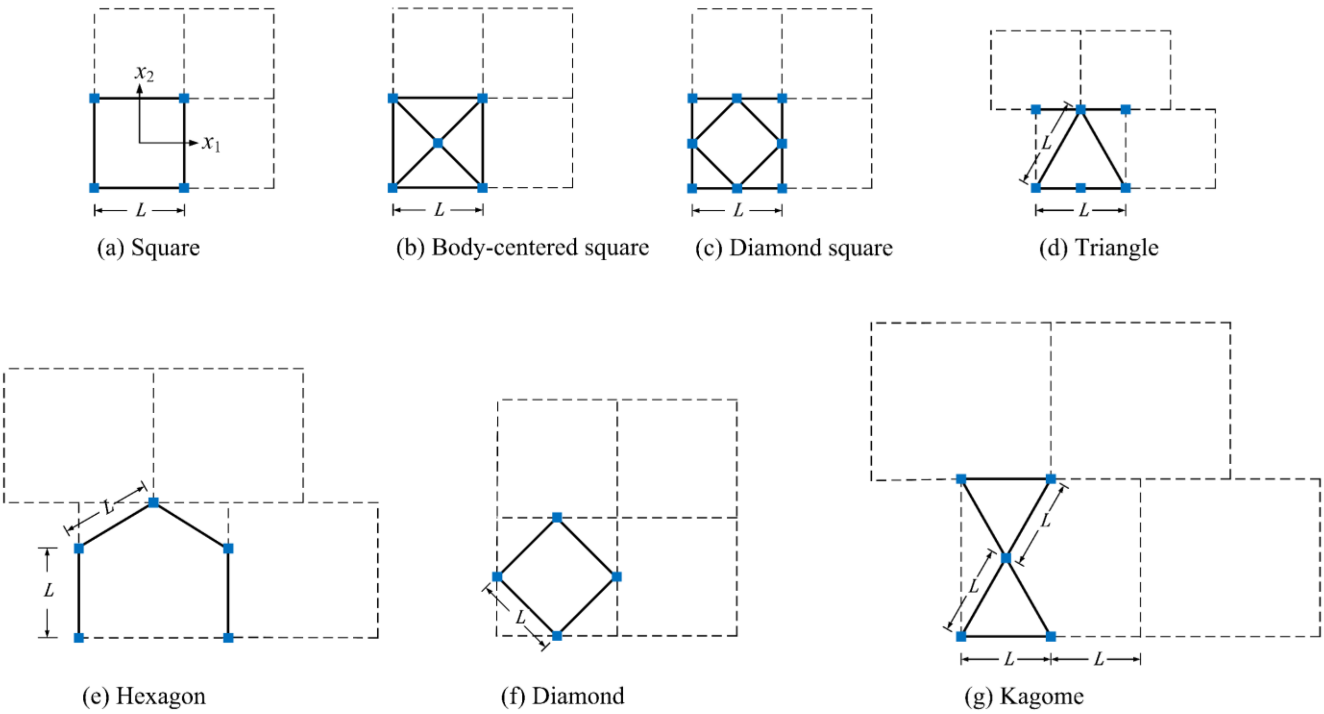

Fig. 2. Considered unit cells.

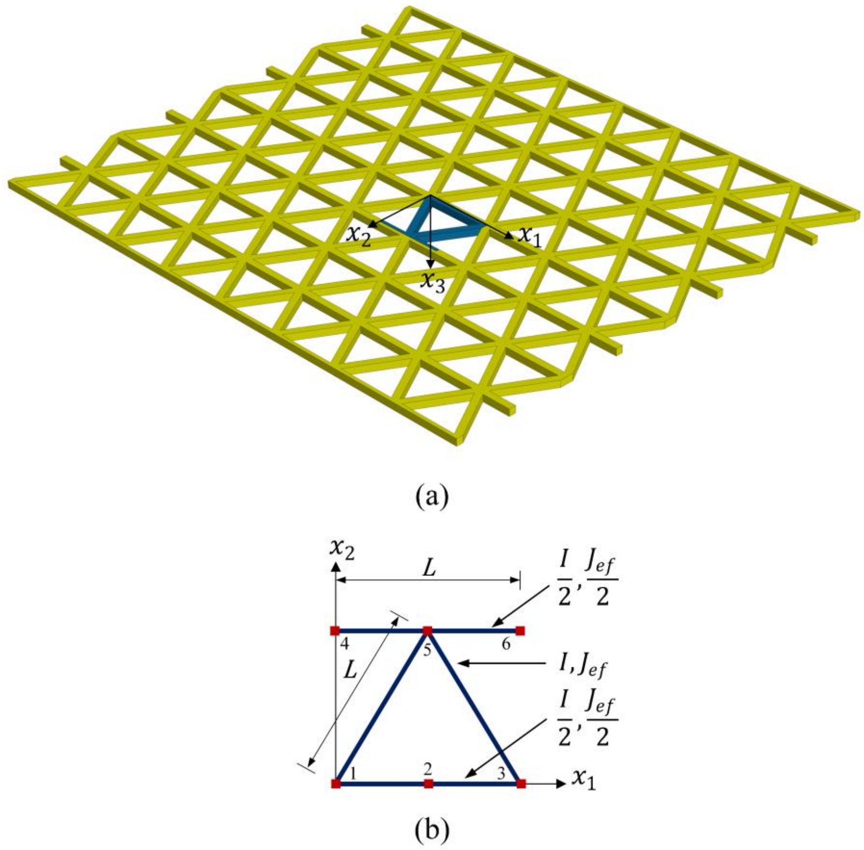

Fig. 3. 2D-lattice plate made of frame-like triangular unit cells: (a) lattice and (b) unit cell.

Table 1. Effective elastic constants of 2D-lattice plates.

Unit cell	E_i^*	ν_{ij}^*	G_{12}^*
Square	$\frac{12EI}{Lh^3}$	0	$\frac{6GJ_{ef}}{Lh^3}$
Body-centered square & Diamond square	$\frac{24EI}{Lh^3}\left[\frac{(\sqrt{2}+1)EI + (\sqrt{2}+2)GJ_{ef}}{(\sqrt{2}+2)EI + \sqrt{2}GJ_{ef}}\right]$	$\frac{EI - GJ_{ef}}{(1+\sqrt{2})EI + GJ_{ef}}$	$\frac{6}{Lh^3}\left[\sqrt{2}EI + GJ_{ef}\right]$
Hexagon	$\frac{16\sqrt{3}EI}{Lh^3}\left[\frac{GJ_{ef}}{EI + 3GJ_{ef}}\right]$	$\frac{EI - GJ_{ef}}{EI + 3GJ_{ef}}$	$\frac{4\sqrt{3}EI}{Lh^3}\left[\frac{GJ_{ef}}{EI + GJ_{ef}}\right]$
Diamond	$\frac{24EI}{Lh^3}\left[\frac{GJ_{ef}}{EI + GJ_{ef}}\right]$	$\frac{EI - GJ_{ef}}{EI + GJ_{ef}}$	$\frac{6EI}{Lh^3}$
Triangle	$\frac{24\sqrt{3}EI}{Lh^3}\left[\frac{EI + GJ_{ef}}{3EI + GJ_{ef}}\right]$	$\frac{EI - GJ_{ef}}{3EI + GJ_{ef}}$	$\frac{3\sqrt{3}}{Lh^3}\left[EI + GJ_{ef}\right]$
Kagome	$\frac{12\sqrt{3}EI}{Lh^3}\left[\frac{EI + GJ_{ef}}{3EI + GJ_{ef}}\right]$	$\frac{EI - GJ_{ef}}{3EI + GJ_{ef}}$	$\frac{3\sqrt{3}}{2Lh^3}\left[EI + GJ_{ef}\right]$

Table 2. Effective elastic constants of 2D-lattice plates with circular and rectangular struts.

Unit cell	E_i^*	ν_{12}^*	G_{12}^*
Square (C)	$\frac{3E\pi D}{16L}$	0	$\frac{3G\pi D}{16L}$
Square (R)	$\frac{EB}{L}$	0	$\frac{GB}{L}\left[6\bar{k}\right]$
Body-centered square (C) & Diamond square (C)	$\frac{3E\pi D}{8L}\left[\frac{(2\sqrt{2}+3)+(\sqrt{2}+1)\nu}{(2\sqrt{2}+2)+(\sqrt{2}+2)\nu}\right]$	$\frac{\sqrt{2}\nu}{(2\sqrt{2}+2)+(\sqrt{2}+2)\nu}$	$\frac{3G\pi D}{16L}\left[(\sqrt{2}+1)+\sqrt{2}\nu\right]$
Body-centered square (R) & Diamond square (R)	$\frac{2EB}{L}\left[\frac{(\sqrt{2}+1)(1+\nu) + (6\sqrt{2}+12)\bar{k}}{(\sqrt{2}+2)(1+\nu) + 6\sqrt{2}\bar{k}}\right]$	$\frac{(1+\nu)-6\bar{k}}{(\sqrt{2}+1)(1+\nu) + 6\bar{k}}$	$\frac{GB}{L}\left[\sqrt{2}(1+\nu)+6\bar{k}\right]$
Hexagon (C)	$\frac{\sqrt{3}E\pi D}{4L}\left[\frac{1}{4+\nu}\right]$	$\frac{\nu}{4+\nu}$	$\frac{\sqrt{3}G\pi D}{8L}\left[\frac{1+\nu}{2+\nu}\right]$
Hexagon (R)	$\frac{4\sqrt{3}EB}{3L}\left[\frac{6\bar{k}}{(1+\nu) + 18\bar{k}}\right]$	$\frac{(1+\nu)-6\bar{k}}{(1+\nu) + 18\bar{k}}$	$\frac{4\sqrt{3}GB}{L}\left[\frac{(1+\nu)\bar{k}}{(1+\nu) + 6\bar{k}}\right]$
Diamond (C)	$\frac{3E\pi D}{8L}\left[\frac{1}{2+\nu}\right]$	$\frac{\nu}{2+\nu}$	$\frac{3G\pi D}{16L}\left[1+\nu\right]$
Diamond (R)	$\frac{2EB}{L}\left[\frac{6\bar{k}}{(1+\nu) + 6\bar{k}}\right]$	$\frac{(1+\nu)-6\bar{k}}{(1+\nu) + 6\bar{k}}$	$\frac{GB}{L}\left[1+\nu\right]$
Triangle (C)	$\frac{3\sqrt{3}E\pi D}{8L}\left[\frac{2+\nu}{4+3\nu}\right]$	$\frac{\nu}{4+3\nu}$	$\frac{3\sqrt{3}G\pi D}{32L}\left[2+\nu\right]$
Triangle (R)	$\frac{2\sqrt{3}EB}{L}\left[\frac{(1+\nu) + 6\bar{k}}{3(1+\nu) + 6\bar{k}}\right]$	$\frac{(1+\nu)-6\bar{k}}{3(1+\nu) + 6\bar{k}}$	$\frac{\sqrt{3}GB}{2L}\left[(1+\nu) + 6\bar{k}\right]$
Kagome (C)	$\frac{3\sqrt{3}E\pi D}{16L}\left[\frac{2+\nu}{4+3\nu}\right]$	$\frac{\nu}{4+3\nu}$	$\frac{3\sqrt{3}G\pi D}{64L}\left[2+\nu\right]$
Kagome (R)	$\frac{\sqrt{3}EB}{L}\left[\frac{(1+\nu) + 6\bar{k}}{3(1+\nu) + 6\bar{k}}\right]$	$\frac{(1+\nu)-6\bar{k}}{3(1+\nu) + 6\bar{k}}$	$\frac{\sqrt{3}GB}{4L}\left[(1+\nu) + 6\bar{k}\right]$

Note: (C) and (R) denote, respectively, circular and rectangular struts.

In this study, 2D-lattice plates with circular and rectangular struts are employed to explain the concept of the proposed design method. Therefore, the solutions in Table 1 are used to compute the effective elastic constants of the considered 2D-lattice plates with circular and rectangular struts. The obtained results are shown in Table 2. In the table, (C) and (R) denote, respectively, circular and rectangular struts. The diameters of circular struts are denoted by D, while the widths and heights of rectangular struts are denoted, respectively, by B and H, as shown in Fig. 4. The thickness of plates with circular struts is taken as D, while the thickness of plates with rectangular struts is taken as H. For the calculation of the torsional stiffness of a $B \times H$ rectangular strut, the effective polar moment of inertia is taken as $J_{ef} = \bar{k}BH^3$, where $\bar{k} = k_1$ when $H \leq B$, and $\bar{k} = k_1 B^2/H^2$ when $H > B$. The coefficient k_1 is a function of the aspect ratio of the rectangular cross-section under consideration. A way to determine k_1 can be found in the work by Timoshenko and Goodier [40]. Since $\bar{k}$ is a function of k_1, it follows that $\bar{k}$ is also a function of the aspect ratio of the rectangular cross-section. Some example values of k_1 are shown in Fig. 4. In Table 2, the closed forms of E_i^* are written as functions of E and ν, while those of G_{12}^* are written in terms of G and ν. In addition, the closed forms of ν_{12}^* are written in terms of ν. It can be seen that E_i^* and G_{12}^* are directly proportional to a sectional dimension, D or B, and are inversely proportional to the unit-cell characteristic length L. With rectangular struts, the effective elastic constants generally vary with the aspect ratio of the strut cross-sections via the coefficient $\bar{k}$. This is because the aspect ratio of the strut cross-sections affects the torsional rigidities of the struts, which in turn affect the values of the effective elastic constants.

Table 3 shows the effective bending and torsional rigidities of the considered 2D-lattice plates with circular and rectangular struts. In the table, the effective bending rigidities R_{bi}^* are written in terms of E, ν, D, B, H, and L, while the effective torsional rigidities R_{t12}^* are given in terms of G, ν, D, B, H, and L. As expected, the effective rigidities always increase when D, B, or H is increased. The effective rigidities are proportional to the fourth-order product of these sectional dimensions. The effective rigidities are inversely proportional to L. With rectangular struts, the effective rigidities are generally found to vary with the aspect ratio of the strut cross-sections via the coefficient $\bar{k}$.

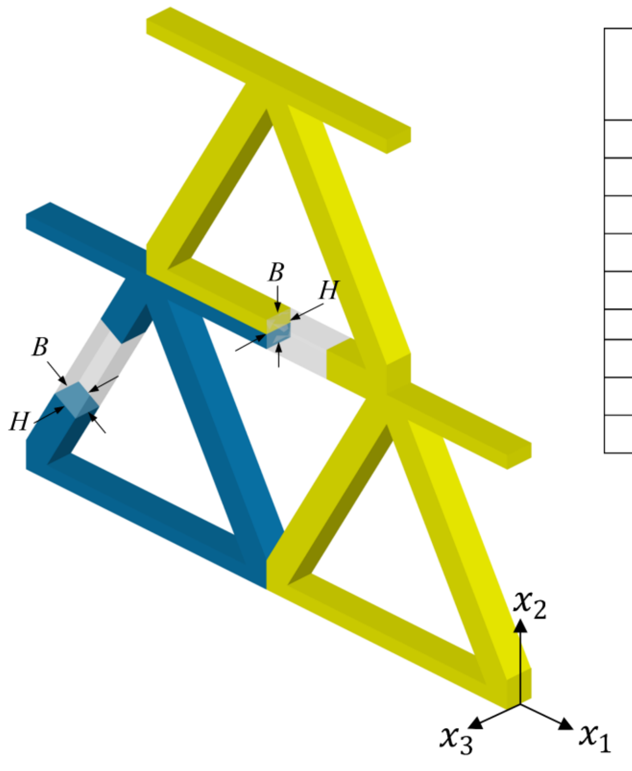

$\frac{a}{b}, a \geq b$	k_1
1.0	0.140577
1.5	0.195761
2.0	0.228682
3.0	0.263317
4.0	0.280813
5.0	0.291317
8.0	0.307073
10.0	0.312325
∞	0.333333

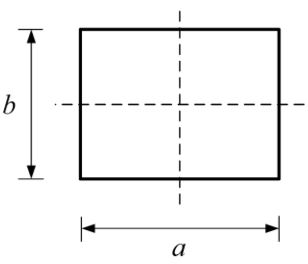

Fig. 4. 2D-lattice plate with rectangular struts.

DOI:10.4186/ej. 2021.25.11.13

Table 3. Effective bending and torsional rigidities of 2D-lattice plates with circular and rectangular struts.

Unit cell	$R_{bi}^* = \dfrac{E_i^* h^3}{12}$	$R_{t12}^* = \dfrac{G_{12}^* h^3}{12}$
Square (C)	$\dfrac{E\pi D^4}{64L}$	$\dfrac{G\pi D^4}{64L}$
Square (R)	$\dfrac{EBH^3}{12L}$	$\dfrac{G\bar{k}BH^3}{2L}$
Body-centered square (C) & Diamond square (C)	$\dfrac{E\pi D^4}{32L}\left[\dfrac{(2\sqrt{2}+3)+(\sqrt{2}+1)\nu}{(2\sqrt{2}+2)+(\sqrt{2}+2)\nu}\right]$	$\dfrac{G\pi D^4}{64L}\left[(\sqrt{2}+1)+\sqrt{2}\nu\right]$
Body-centered square (R) & Diamond square (R)	$\dfrac{EBH^3}{6L}\left[\dfrac{(\sqrt{2}+1)(1+\nu)+(6\sqrt{2}+12)\bar{k}}{(\sqrt{2}+2)(1+\nu)+6\sqrt{2}\bar{k}}\right]$	$\dfrac{GBH^3}{12L}\left[\sqrt{2}(1+\nu)+6\bar{k}\right]$
Hexagon (C)	$\dfrac{\sqrt{3}E\pi D^4}{48L}\left[\dfrac{1}{4+\nu}\right]$	$\dfrac{\sqrt{3}G\pi D^4}{96L}\left[\dfrac{1+\nu}{2+\nu}\right]$
Hexagon (R)	$\dfrac{2\sqrt{3}EBH^3}{3L}\left[\dfrac{\bar{k}}{1+\nu+18\bar{k}}\right]$	$\dfrac{\sqrt{3}GBH^3}{3L}\left[\dfrac{(1+\nu)\bar{k}}{1+\nu+6\bar{k}}\right]$
Diamond (C)	$\dfrac{E\pi D^4}{32L}\left[\dfrac{1}{2+\nu}\right]$	$\dfrac{G\pi D^4}{64L}[1+\nu]$
Diamond (R)	$\dfrac{EBH^3}{L}\left[\dfrac{\bar{k}}{1+\nu+6\bar{k}}\right]$	$\dfrac{GBH^3}{12L}[1+\nu]$
Triangle (C)	$\dfrac{\sqrt{3}E\pi D^4}{32L}\left[\dfrac{2+\nu}{4+3\nu}\right]$	$\dfrac{\sqrt{3}G\pi D^4}{128L}[2+\nu]$
Triangle (R)	$\dfrac{\sqrt{3}EBH^3}{6L}\left[\dfrac{(1+\nu)+6\bar{k}}{3(1+\nu)+6\bar{k}}\right]$	$\dfrac{\sqrt{3}GBH^3}{24L}\left[1+\nu+6\bar{k}\right]$
Kagome (C)	$\dfrac{\sqrt{3}E\pi D^4}{64L}\left[\dfrac{2+\nu}{4+3\nu}\right]$	$\dfrac{\sqrt{3}G\pi D^4}{256L}[2+\nu]$
Kagome (R)	$\dfrac{\sqrt{3}EBH^3}{36L}\left[\dfrac{1+\nu+6\bar{k}}{1+\nu+2\bar{k}}\right]$	$\dfrac{\sqrt{3}GBH^3}{48L}\left[1+\nu+6\bar{k}\right]$

Note: (C) and (R) denote, respectively, circular and rectangular struts.

6. Design Method for Weight Efficiency and Example Design Graphs

To design 2D-lattice plates by targeting their weight efficiency, the relationships between the effective rigidities and the area weight densities of the plates can be considered. These relationships are obtained through the expressions of the effective rigidities per area weight density R_{bi}^*/ρ_A^* and R_{t12}^*/ρ_A^*. In addition, the efficiency of unit-cell patterns in terms of the weight efficiency of their resulting plates is obtained through the expressions of the normalized specific effective rigidities $\hat{Z}_{bi}^*$ and $\hat{Z}_{t12}^*$.Table 4 shows the volume fractions V_f and the area weight densities ρ_A^* of the considered 2D-lattice plates. For easy presentation, the area weight densities ρ_A^* are normalized by the weight density of the base material ρ. From the expressions of the effective rigidities in Table 3 and the normalized area weight densities in Table 4, the relationships between the effective rigidities and the normalized area weight densities can be found.

Table 5 shows the closed-form effective rigidities per area weight density R_{bi}^*/ρ_A^* and R_{t12}^*/ρ_A^*. The table also shows the closed-form normalized specific effective rigidities $\hat{Z}_{bi}^*$ and $\hat{Z}_{t12}^*$. It can be seen that $\hat{Z}_{bi}^*$ and $\hat{Z}_{t12}^*$ are functions of ν except for square unit cells. In addition, in most cases of rectangular struts, $\hat{Z}_{bi}^*$ and $\hat{Z}_{t12}^*$ vary with the aspect ratio of the strut cross-sections via the coefficient $\bar{k}$. As mentioned above, the normalized specific effective rigidities $\hat{Z}_{bi}^*$ and $\hat{Z}_{t12}^*$ can be used to compare the efficiency of unit-cell patterns in terms of the weight efficiency of their resulting plates. For example, if Poisson's ratio of the base material ν is equal to $1/3$, from Table 5, $\hat{Z}_{b1}^*$ and $\hat{Z}_{b2}^*$ of 2D-lattice plates having triangular unit cells with circular struts are found to be equal to 0.35.

In addition, $\hat{Z}^*_{b1}$ and $\hat{Z}^*_{b2}$ of 2D-lattice plates having square unit cells with circular struts are found to be equal to 0.375. This means that, for bending rigidities, the square unit-cell pattern yields better weight efficiency of 2D-lattice plates than the triangular unit-cell pattern when $\nu = 1/3$. If a material having $\nu = 1/3$ is used to create different plates that have the same thickness and the same area weight density, those plates having square unit cells with circular struts will have higher effective bending rigidities than those having triangular unit cells with circular struts.

From the relationships between the effective rigidities and the normalized area weight densities in Table 5, the normalized area weight densities are written in terms of the effective rigidities in Table 6 and Table 7. These expressions of the normalized area weight densities written in terms of the effective rigidities enable the weight efficiency of different 2D-lattice plates designed for the same rigidities to be compared. In Table 6, the normalized area weight densities ρ^*_A/ρ are written in terms of the effective bending rigidity R^*_{b1}, which is equal to R^*_{b2}. In addition, in Table 6, three forms of the normalized area weight densities are presented. Except for R^*_{b1}, these forms have different input parameters for different design requirements. For example, to design a 2D-lattice plate with rectangular struts, for a required value of R^*_{b1}, it may be necessary to first specify the height H of rectangular struts. In this case, the formulas, whose input parameters are R^*_{b1} and H, can be used to compute the area weight densities ρ^*_A for different designs, which may include different unit-cell geometry or different materials or both. The obtained area weight densities ρ^*_A for different designs can then be compared. After the design with the lowest ρ^*_A is selected, the values of H and its ρ^*_A/ρ can then be used to select B and L, which must satisfy the relationship, $\rho^*_A/\rho = 2BH/L$, in Table 4. For the cases of circular struts, the input parameters in Table 6, in addition to R^*_{b1}, are

- D, or
- D/L, or
- L.

For the cases of rectangular struts, the input parameters, in addition to R^*_{b1}, are

- H, or
- H/L and $\beta = B/H$, or
- L and β.

Similarly, in Table 7, the normalized area weight densities ρ^*_A/ρ are written in terms of the effective torsional rigidity R^*_{t12}.

Table 4. Volume fractions and normalized area weight densities of 2D-lattice plates.

Unit cell	Volume fraction V_f		Normalized area weight density, $\rho^*_A/\rho = V_f h$	
	(C)	(R)	(C)	(R)
Square	$\frac{\pi D}{2L}$	$\frac{2B}{L}$	$\frac{\pi D^2}{2L}$	$\frac{2BH}{L}$
Body-centered square & Diamond square	$\frac{(\sqrt{2}+1)\pi D}{2L}$	$\frac{2(\sqrt{2}+1)B}{L}$	$\frac{(\sqrt{2}+1)\pi D^2}{2L}$	$\frac{2(\sqrt{2}+1)BH}{L}$
Hexagon	$\frac{\sqrt{3}\pi D}{6L}$	$\frac{2\sqrt{3}B}{3L}$	$\frac{\sqrt{3}\pi D^2}{6L}$	$\frac{2\sqrt{3}BH}{3L}$
Diamond	$\frac{\pi D}{2L}$	$\frac{2B}{L}$	$\frac{\pi D^2}{2L}$	$\frac{2BH}{L}$
Triangle	$\frac{\sqrt{3}\pi D}{2L}$	$\frac{2\sqrt{3}B}{L}$	$\frac{\sqrt{3}\pi D^2}{2L}$	$\frac{2\sqrt{3}BH}{L}$
Kagome	$\frac{\sqrt{3}\pi D}{4L}$	$\frac{\sqrt{3}B}{L}$	$\frac{\sqrt{3}\pi D^2}{4L}$	$\frac{\sqrt{3}BH}{L}$

Note: (C) and (R) denote, respectively, circular and rectangular struts.

DOI:10.4186/ej. 2021.25.11.13

Table 5. Relationships between the effective rigidities and the area weight densities, and the normalized specific effective rigidities of 2D-lattice plates with circular and rectangular struts.

Unit cell	$\frac{R_{bi}^*}{\rho_A^*}$	$\frac{R_{t12}^*}{\rho_A^*}$	$\hat{Z}_{bi}^*$	$\hat{Z}_{t12}^*$
Square (C)	$\frac{ED^2}{32\rho}$	$\frac{GD^2}{32\rho}$	$\frac{3}{8}$	$\frac{3}{8}$
Square (R)	$\frac{EH^2}{24\rho}$	$\frac{G\bar{k}H^2}{4\rho}$	$\frac{1}{2}$	$3\bar{k}$
Body-centered square (C) & Diamond square (C)	$\frac{ED^2}{16\rho(\sqrt{2}+1)}\left[\frac{(2\sqrt{2}+3)+(\sqrt{2}+1)\nu}{(2\sqrt{2}+2)\ +(\sqrt{2}+2)\nu}\right]$	$\frac{GD^2}{32\rho(\sqrt{2}+1)}\left[(\sqrt{2}+1)+\sqrt{2}\nu\right]$	$\frac{3}{4(\sqrt{2}+1)}\left[\frac{(2\sqrt{2}+3)+(\sqrt{2}+1)\nu}{(2\sqrt{2}+2)\ +(\sqrt{2}+2)\nu}\right]$	$\frac{3}{8(\sqrt{2}+1)}\left[(\sqrt{2}+1)+\sqrt{2}\nu\right]$
Body-centered square (R) & Diamond square (R)	$\frac{EH^2}{12\rho(\sqrt{2}+1)}\left[\frac{(\sqrt{2}+1)(1+\nu)+\ (\sqrt{2}+2)6\bar{k}}{(\sqrt{2}+2)(1+\nu)\ +\ 6\sqrt{2}\bar{k}}\right]$	$\frac{GH^2}{24\rho(\sqrt{2}+1)}\left[\sqrt{2}(1+\nu)+6\bar{k}\right]$	$\frac{1}{(\sqrt{2}+1)}\left[\frac{(\sqrt{2}+1)(1+\nu)+\ (\sqrt{2}+2)6\bar{k}}{(\sqrt{2}+2)(1+\nu)\ +\ 6\sqrt{2}\bar{k}}\right]$	$\frac{1}{2(\sqrt{2}+1)}\left[\sqrt{2}(1+\nu)+6\bar{k}\right]$
Hexagon (C)	$\frac{ED^2}{8\rho}\left[\frac{1}{4+\nu}\right]$	$\frac{GD^2}{16\rho}\left[\frac{1+\nu}{2+\nu}\right]$	$\frac{3}{2}\left[\frac{1}{4+\nu}\right]$	$\frac{3}{4}\left[\frac{1+\nu}{2+\nu}\right]$
Hexagon (R)	$\frac{EH^2}{3\rho}\left[\frac{\bar{k}}{\frac{1}{3}(1+\nu)+\ 6\bar{k}}\right]$	$\frac{GH^2}{2\rho}\left[\frac{(1+\nu)\bar{k}}{(1+\nu)+\ 6\bar{k}}\right]$	$\frac{4\bar{k}}{\frac{1}{3}(1+\nu)+\ 6\bar{k}}$	$\frac{(1+\nu)6\bar{k}}{(1+\nu)+\ 6\bar{k}}$
Diamond (C)	$\frac{ED^2}{16\rho}\left[\frac{1}{2+\nu}\right]$	$\frac{GD^2}{32\rho}[1+\nu]$	$\frac{3}{4}\left[\frac{1}{2+\nu}\right]$	$\frac{3}{8}[1+\nu]$
Diamond (R)	$\frac{EH^2}{2\rho}\left[\frac{\bar{k}}{(1+\nu)+\ 6\bar{k}}\right]$	$\frac{GH^2}{24\rho}[1+\nu]$	$\frac{6\bar{k}}{(1+\nu)+\ 6\bar{k}}$	$\frac{1}{2}[1+\nu]$
Triangle (C)	$\frac{ED^2}{16\rho}\left[\frac{2+\nu}{4+3\nu}\right]$	$\frac{GD^2}{64\rho}[2+\nu]$	$\frac{3}{4}\left[\frac{2+\nu}{4+3\nu}\right]$	$\frac{3}{16}[2+\nu]$
Triangle (R)	$\frac{EH^2}{12\rho}\left[\frac{(1+\nu)+\ 6\bar{k}}{3(1+\nu)+\ 6\bar{k}}\right]$	$\frac{GH^2}{48\rho}\left[(1+\nu)+\ 6\bar{k}\right]$	$\frac{(1+\nu)+\ 6\bar{k}}{3(1+\nu)+\ 6\bar{k}}$	$\frac{1}{4}\left[(1+\nu)+\ 6\bar{k}\right]$
Kagome (C)	$\frac{ED^2}{16\rho}\left[\frac{2+\nu}{4+3\nu}\right]$	$\frac{GD^2}{64\rho}[2+\nu]$	$\frac{3}{4}\left[\frac{2+\nu}{4+3\nu}\right]$	$\frac{3}{16}[2+\nu]$
Kagome (R)	$\frac{EH^2}{12\rho}\left[\frac{(1+\nu)+\ 6\bar{k}}{3(1+\nu)+\ 6\bar{k}}\right]$	$\frac{GH^2}{48\rho}\left[(1+\nu)+\ 6\bar{k}\right]$	$\frac{(1+\nu)+\ 6\bar{k}}{3(1+\nu)+\ 6\bar{k}}$	$\frac{1}{4}\left[(1+\nu)+\ 6\bar{k}\right]$

Note: (C) and (R) denote, respectively, circular and rectangular struts

Table 6. Normalized area weight densities of 2D-lattice plates with circular and rectangular struts, in terms of the effective bending rigidities.

Unit cell	$\frac{\rho_A^*}{\rho}(R_{b1}^*, D)$ for (C), $\frac{\rho_A^*}{\rho}(R_{b1}^*, H)$ for (R)	$\frac{\rho_A^*}{\rho}\left(R_{b1}^*, \frac{D}{L}\right)$ for (C), $\frac{\rho_A^*}{\rho}\left(R_{b1}^*, \frac{H}{L}, \beta\right)$ for (R)	$\frac{\rho_A^*}{\rho}(R_{b1}^*, L)$ for (C), $\frac{\rho_A^*}{\rho}(R_{b1}^*, L, \beta)$ for (R)
Square (C)	$\frac{32R_{b1}^*}{ED^2}$	$\left[\frac{8R_{b1}^*\pi^2}{E}\left(\frac{D}{L}\right)^2\right]^{\frac{1}{3}}$	$\left[\frac{16R_{b1}^*\pi}{EL}\right]^{\frac{1}{2}}$
Square (R)	$\frac{24R_{b1}^*}{EH^2}$	$\left[\frac{96R_{b1}^*\beta^2}{E}\left(\frac{H}{L}\right)^2\right]^{\frac{1}{3}}$	$\left[\frac{48R_{b1}^*\beta}{EL}\right]^{\frac{1}{2}}$
Body-centered square (C) & Diamond square (C)	$\frac{16R_{b1}^*(\sqrt{2}+1)}{ED^2}\left[\frac{(2\sqrt{2}+2)+(\sqrt{2}+2)\nu}{(2\sqrt{2}+3)+(\sqrt{2}+1)\nu}\right]$	$\left[\frac{4R_{b1}^*\pi^2(\sqrt{2}+1)^3}{E}\left[\frac{(2\sqrt{2}+2)+(\sqrt{2}+2)\nu}{(2\sqrt{2}+3)+(\sqrt{2}+1)\nu}\right]\left(\frac{D}{L}\right)^2\right]^{\frac{1}{3}}$	$\left[\frac{8R_{b1}^*\pi(\sqrt{2}+1)^2}{EL}\left[\frac{(2\sqrt{2}+2)+(\sqrt{2}+2)\nu}{(2\sqrt{2}+3)+(\sqrt{2}+1)\nu}\right]\right]^{\frac{1}{2}}$
Body-centered square (R) & Diamond square (R)	$\frac{12R_{b1}^*(\sqrt{2}+1)}{EH^2}\left[\frac{(\sqrt{2}+2)(1+\nu)+6\sqrt{2}\bar{k}}{(\sqrt{2}+1)(1+\nu)+(\sqrt{2}+2)6\bar{k}}\right]$	$\left[\frac{48R_{b1}^*\beta^2(\sqrt{2}+1)^3}{E}\left[\frac{(\sqrt{2}+2)(1+\nu)+6\sqrt{2}\bar{k}}{(\sqrt{2}+1)(1+\nu)+(\sqrt{2}+2)6\bar{k}}\right]\left(\frac{H}{L}\right)^2\right]^{\frac{1}{3}}$	$\left[\frac{24R_{b1}^*\beta(\sqrt{2}+1)^2}{EL}\left[\frac{(\sqrt{2}+2)(1+\nu)+6\sqrt{2}\bar{k}}{(\sqrt{2}+1)(1+\nu)+(\sqrt{2}+2)6\bar{k}}\right]\right]^{\frac{1}{2}}$
Hexagon (C)	$\frac{8R_{b1}^*[4+\nu]}{ED^2}$	$\left[\frac{2R_{b1}^*\pi^2[4+\nu]}{3E}\left(\frac{D}{L}\right)^2\right]^{\frac{1}{3}}$	$\left[\frac{4\sqrt{3}R_{b1}^*\pi[4+\nu]}{3EL}\right]^{\frac{1}{2}}$
Hexagon (R)	$\frac{R_{b1}^*}{EH^2}\left[\frac{1+\nu+18\bar{k}}{\bar{k}}\right]$	$\left[\frac{4R_{b1}^*\beta^2}{E}\left[\frac{1+\nu+18\bar{k}}{3\bar{k}}\right]\left(\frac{H}{L}\right)^2\right]^{\frac{1}{3}}$	$\left[\frac{2\sqrt{3}R_{b1}^*\beta}{EL}\left[\frac{1+\nu+18\bar{k}}{3\bar{k}}\right]\right]^{\frac{1}{2}}$
Diamond (C)	$\frac{16R_{b1}^*[2+\nu]}{ED^2}$	$\left[\frac{4R_{b1}^*\pi^2[2+\nu]}{E}\left(\frac{D}{L}\right)^2\right]^{\frac{1}{3}}$	$\left[\frac{8R_{b1}^*\pi[2+\nu]}{EL}\right]^{\frac{1}{2}}$
Diamond (R)	$\frac{2R_{b1}^*}{EH^2}\left[\frac{1+\nu+6\bar{k}}{\bar{k}}\right]$	$\left[\frac{8R_{b1}^*\beta^2}{E}\left[\frac{1+\nu+6\bar{k}}{\bar{k}}\right]\left(\frac{H}{L}\right)^2\right]^{\frac{1}{3}}$	$\left[\frac{4R_{b1}^*\beta}{EL}\left[\frac{1+\nu+6\bar{k}}{\bar{k}}\right]\right]^{\frac{1}{2}}$
Triangle (C)	$\frac{16R_{b1}^*}{ED^2}\left[\frac{4+3\nu}{2+\nu}\right]$	$\left[\frac{12R_{b1}^*\pi^2}{E}\left[\frac{4+3\nu}{2+\nu}\right]\left(\frac{D}{L}\right)^2\right]^{\frac{1}{3}}$	$\left[\frac{8\sqrt{3}R_{b1}^*\pi}{EL}\left[\frac{4+3\nu}{2+\nu}\right]\right]^{\frac{1}{2}}$
Triangle (R)	$\frac{36R_{b1}^*}{EH^2}\left[\frac{1+\nu+2\bar{k}}{1+\nu+6\bar{k}}\right]$	$\left[\frac{432R_{b1}^*\beta^2}{E}\left[\frac{1+\nu+2\bar{k}}{1+\nu+6\bar{k}}\right]\left(\frac{H}{L}\right)^2\right]^{\frac{1}{3}}$	$\left[\frac{72\sqrt{3}R_{b1}^*\beta}{EL}\left[\frac{1+\nu+2\bar{k}}{1+\nu+6\bar{k}}\right]\right]^{\frac{1}{2}}$
Kagome (C)	$\frac{16R_{b1}^*}{ED^2}\left[\frac{4+3\nu}{2+\nu}\right]$	$\left[\frac{3R_{b1}^*\pi^2}{E}\left[\frac{4+3\nu}{2+\nu}\right]\left(\frac{D}{L}\right)^2\right]^{\frac{1}{3}}$	$\left[\frac{4\sqrt{3}R_{b1}^*\pi}{EL}\left[\frac{4+3\nu}{2+\nu}\right]\right]^{\frac{1}{2}}$
Kagome (R)	$\frac{36R_{b1}^*}{EH^2}\left[\frac{1+\nu+2\bar{k}}{1+\nu+6\bar{k}}\right]$	$\left[\frac{108R_{b1}^*\beta^2}{E}\left[\frac{1+\nu+2\bar{k}}{1+\nu+6\bar{k}}\right]\left(\frac{H}{L}\right)^2\right]^{\frac{1}{3}}$	$\left[\frac{36\sqrt{3}R_{b1}^*\beta}{EL}\left[\frac{1+\nu+2\bar{k}}{1+\nu+6\bar{k}}\right]\right]^{\frac{1}{2}}$

Note: (C) and (R) denote, respectively, circular and rectangular struts. $\beta = B/H$. $R_{b1}^* = R_{b2}^*$

DOI:10.4186/ej. 2021.25.11.13

Table 7. Normalized area weight densities of 2D-lattice plates with circular and rectangular struts, in terms of the effective torsional rigidities.

Unit cell	$\frac{\rho_A^*}{\rho}(R_{t12}^*, D)$ for (C), $\frac{\rho_A^*}{\rho}(R_{t12}^*, H)$ for (R)	$\frac{\rho_A^*}{\rho}\left(R_{t12}^*, \frac{D}{L}\right)$ for (C), $\frac{\rho_A^*}{\rho}\left(R_{t12}^*, \frac{H}{L}, \beta\right)$ for (R)	$\frac{\rho_A^*}{\rho}(R_{t12}^*, L)$ for (C), $\frac{\rho_A^*}{\rho}(R_{t12}^*, L, \beta)$ for (R)
Square (C)	$\frac{32R_{t12}^*}{GD^2}$	$\left[\frac{8R_{t12}^*\pi^2}{G}\left(\frac{D}{L}\right)^2\right]^{\frac{1}{3}}$	$\left[\frac{16R_{t12}^*\pi}{GL}\right]^{\frac{1}{2}}$
Square (R)	$\frac{4R_{t12}^*}{GH^2\bar{k}}$	$\left[\frac{16R_{t12}^*\beta^2}{G\bar{k}}\left(\frac{H}{L}\right)^2\right]^{\frac{1}{3}}$	$\left[\frac{8R_{t12}^*\beta}{GL\bar{k}}\right]^{\frac{1}{2}}$
Body-centered square (C) & Diamond square (C)	$\frac{32R_{t12}^*(\sqrt{2}+1)}{GD^2[(\sqrt{2}+1)+\sqrt{2}\nu]}$	$\left[\frac{8R_{t12}^*\pi^2(\sqrt{2}+1)^3}{G[(\sqrt{2}+1)+\sqrt{2}\nu]}\left(\frac{D}{L}\right)^2\right]^{\frac{1}{3}}$	$\left[\frac{16R_{t12}^*\pi(\sqrt{2}+1)^2}{GL[(\sqrt{2}+1)+\sqrt{2}\nu]}\right]^{\frac{1}{2}}$
Body-centered square (R) & Diamond square (R)	$\frac{24R_{t12}^*(\sqrt{2}+1)}{GH^2[\sqrt{2}(1+\nu)+6\bar{k}]}$	$\left[\frac{96R_{t12}^*\beta^2(\sqrt{2}+1)^3}{G[\sqrt{2}(1+\nu)+6\bar{k}]}\left(\frac{H}{L}\right)^2\right]^{\frac{1}{3}}$	$\left[\frac{48R_{t12}^*\beta(\sqrt{2}+1)^2}{GL[\sqrt{2}(1+\nu)+6\bar{k}]}\right]^{\frac{1}{2}}$
Hexagon (C)	$\frac{16R_{t12}^*}{GD^2}\left[\frac{2+\nu}{1+\nu}\right]$	$\left[\frac{4R_{t12}^*\pi^2}{3G}\left[\frac{2+\nu}{1+\nu}\right]\left(\frac{D}{L}\right)^2\right]^{\frac{1}{3}}$	$\left[\frac{8\sqrt{3}R_{t12}^*\pi}{3GL}\left[\frac{2+\nu}{1+\nu}\right]\right]^{\frac{1}{2}}$
Hexagon (R)	$\frac{2R_{t12}^*}{GH^2\bar{k}}\left[\frac{1+\nu+6\bar{k}}{1+\nu}\right]$	$\left[\frac{8R_{t12}^*\beta^2}{3G\bar{k}}\left[\frac{1+\nu+6\bar{k}}{1+\nu}\right]\left(\frac{H}{L}\right)^2\right]^{\frac{1}{3}}$	$\left[\frac{4\sqrt{3}R_{t12}^*\beta}{3GL\bar{k}}\left[\frac{1+\nu+6\bar{k}}{1+\nu}\right]\right]^{\frac{1}{2}}$
Diamond (C)	$\frac{32R_{t12}^*}{GD^2[1+\nu]}$	$\left[\frac{8R_{t12}^*\pi^2}{G[1+\nu]}\left(\frac{D}{L}\right)^2\right]^{\frac{1}{3}}$	$\left[\frac{16R_{t12}^*\pi}{GL[1+\nu]}\right]^{\frac{1}{2}}$
Diamond (R)	$\frac{24R_{t12}^*}{GH^2[1+\nu]}$	$\left[\frac{96R_{t12}^*\beta^2}{G[1+\nu]}\left(\frac{H}{L}\right)^2\right]^{\frac{1}{3}}$	$\left[\frac{48R_{t12}^*\beta}{GL[1+\nu]}\right]^{\frac{1}{2}}$
Triangle (C)	$\frac{64R_{t12}^*}{GD^2[2+\nu]}$	$\left[\frac{48R_{t12}^*\pi^2}{G[2+\nu]}\left(\frac{D}{L}\right)^2\right]^{\frac{1}{3}}$	$\left[\frac{32\sqrt{3}R_{t12}^*\pi}{GL[2+\nu]}\right]^{\frac{1}{2}}$
Triangle (R)	$\frac{48R_{t12}^*}{GH^2[1+\nu+6\bar{k}]}$	$\left[\frac{576R_{t12}^*\beta^2}{G[1+\nu+6\bar{k}]}\left(\frac{H}{L}\right)^2\right]^{\frac{1}{3}}$	$\left[\frac{96\sqrt{3}R_{t12}^*\beta}{GL[1+\nu+6\bar{k}]}\right]^{\frac{1}{2}}$
Kagome (C)	$\frac{64R_{t12}^*}{GD^2[2+\nu]}$	$\left[\frac{12R_{t12}^*\pi^2}{G[2+\nu]}\left(\frac{D}{L}\right)^2\right]^{\frac{1}{3}}$	$\left[\frac{16\sqrt{3}R_{t12}^*\pi}{GL[2+\nu]}\right]^{\frac{1}{2}}$
Kagome (R)	$\frac{48R_{t12}^*}{GH^2[1+\nu+6\bar{k}]}$	$\left[\frac{144R_{t12}^*\beta^2}{G[1+\nu+6\bar{k}]}\left(\frac{H}{L}\right)^2\right]^{\frac{1}{3}}$	$\left[\frac{48\sqrt{3}R_{t12}^*\beta}{GL[1+\nu+6\bar{k}]}\right]^{\frac{1}{2}}$

Note: (C) and (R) denote, respectively, circular and rectangular struts. $\beta = B/H$

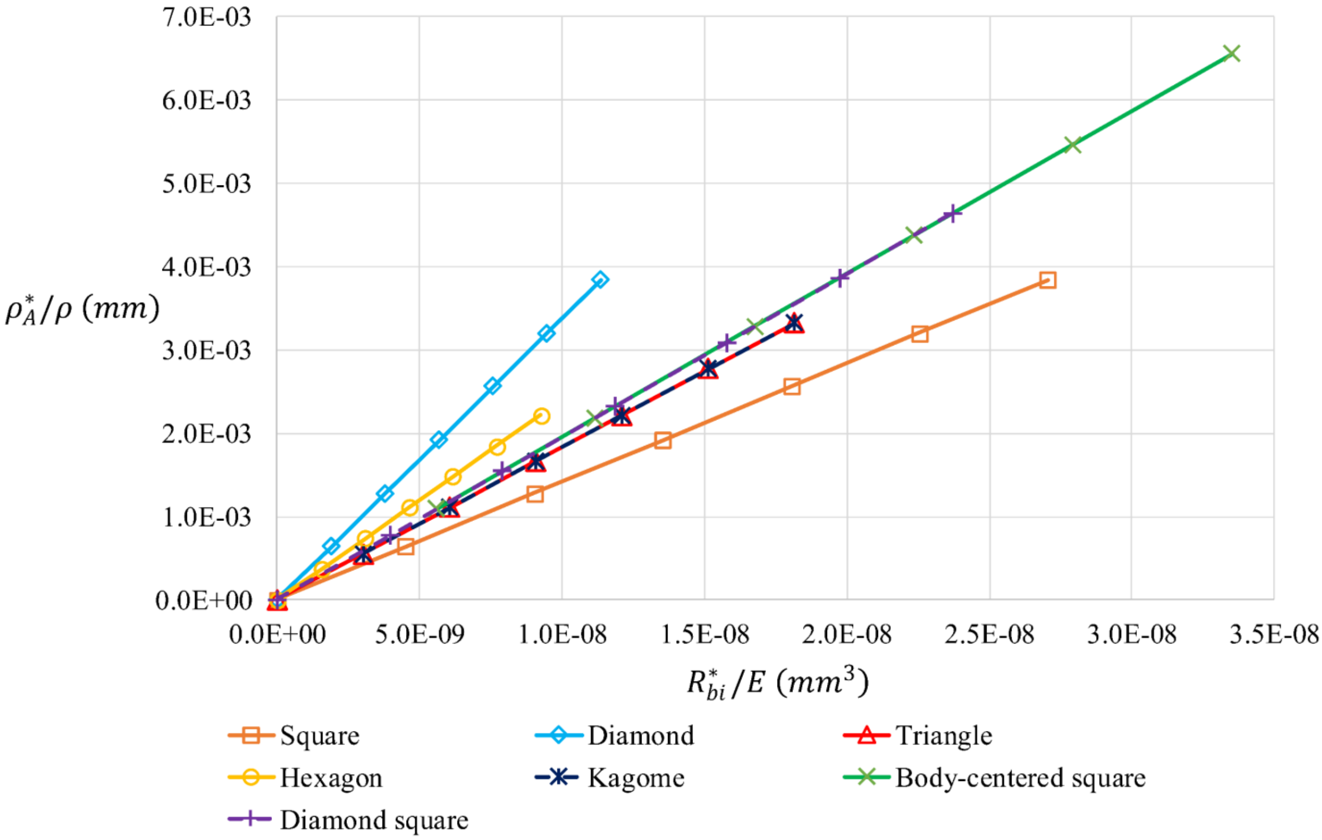

Fig. 5. Relationships between the effective bending rigidities and the normalized area weight densities of 2D-lattice plates with rectangular struts.

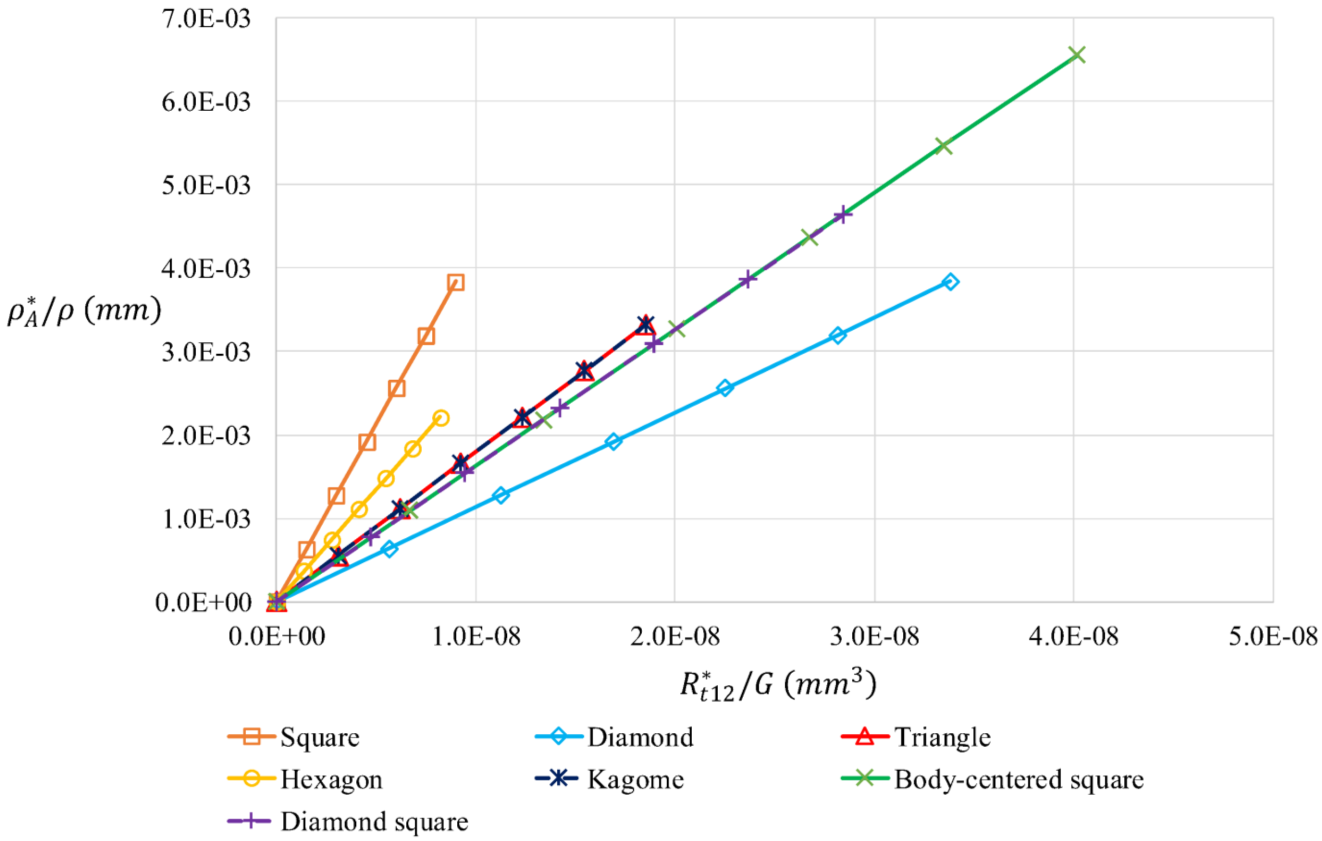

Fig. 6. Relationships between the effective torsional rigidities and the normalized area weight densities of 2D-lattice plates with rectangular struts.

DOI:10.4186/ej. 2021.25.11.13

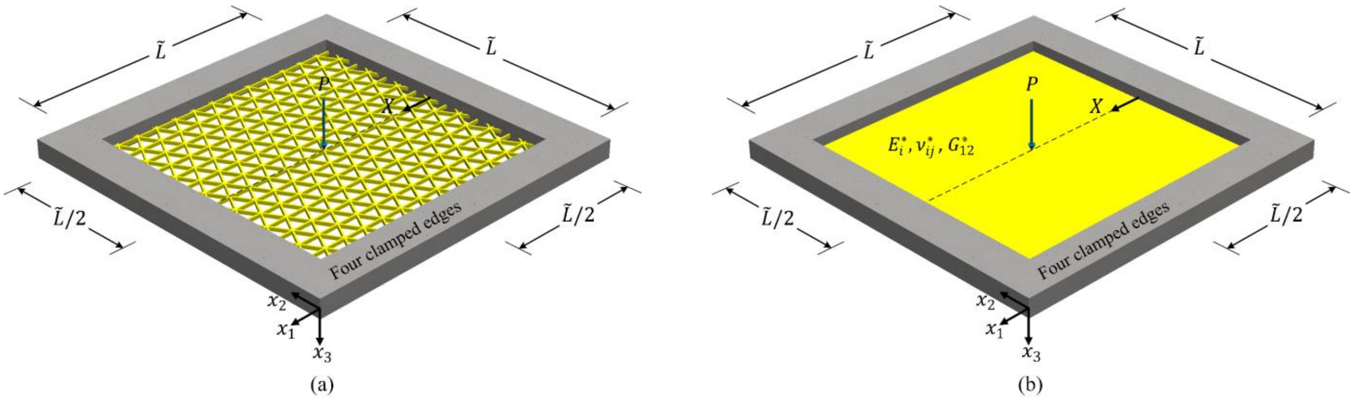

Fig. 7. Clamped square 2D-lattice plate: (a) original lattice and (b) equivalent homogeneous plate.

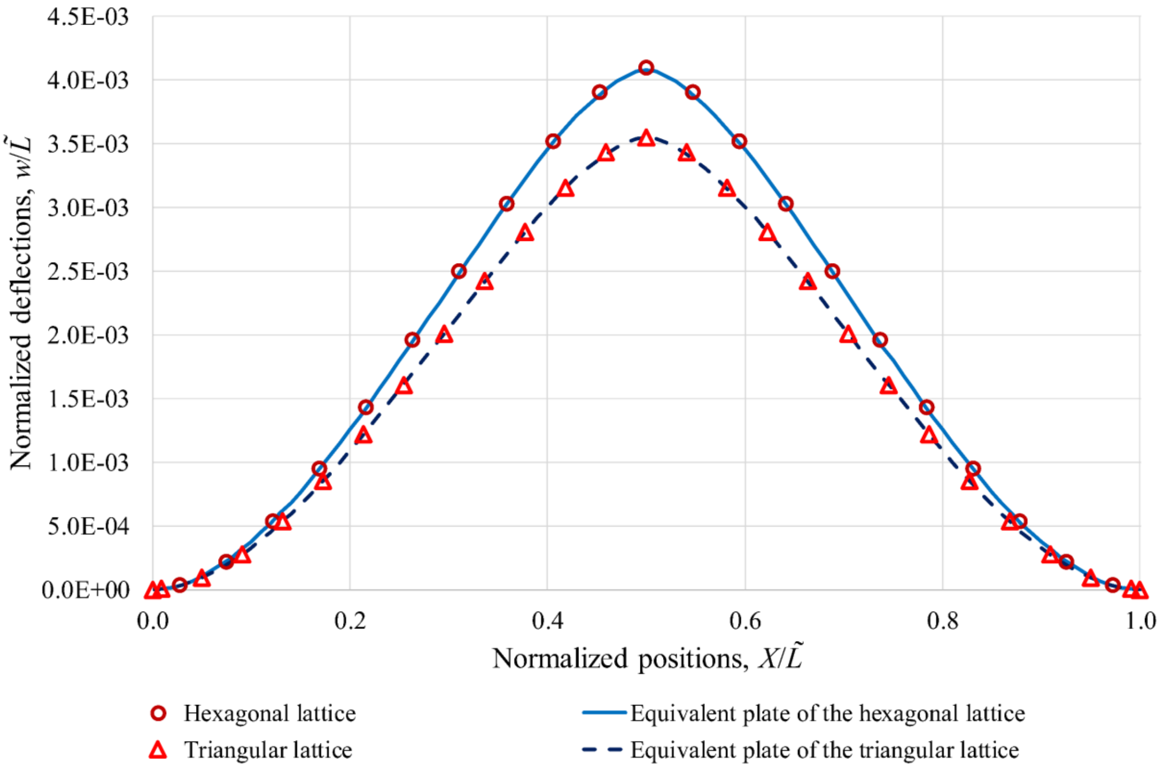

Fig. 8. Normalized deflections of 2D-lattice plates of hexagonal and triangular unit cells.

From a designer's point of view, better unit-cell patterns are those that, for required rigidities, yield lighter weights of the resulting lattices. Fig. 5 and Fig. 6 show examples of design graphs for 2D-lattice plates. The graphs provide the relationships between the effective rigidities, normalized by Young's modulus E or the shear modulus G of the base material, and the area weight densities, normalized by the weight density of the base material. The graphs are constructed for lattices having rectangular struts with $B \times H = 6.40 \times 13.00$ mm and having Poisson's ratio of the base material $\nu = 0.25$. Note that the chosen strut sectional dimensions are taken from an existing floor grating product. From these design graphs, the normalized area weight densities for any required rigidities can be determined for lattices constructed from different unit-cell patterns. The graphs are constructed from the formulas of $\rho_A^*/\rho(R_{b1}^*, H)$ in Table 6, and $\rho_A^*/\rho(R_{t12}^*, H)$ in Table 7. To achieve the required rigidities, the characteristic length L needs to be adjusted. Its value can be determined via the values of ρ_A^*/ρ, B, H, and the expressions of $\rho_A^*/\rho(B, H, L)$ in Table 4. It can be seen from Table 6 and Table 7 that $\rho_A^*/\rho(R_{b1}^*, H)$ and $\rho_A^*/\rho(R_{t12}^*, H)$ vary linearly, respectively, with R_{b1}^* and R_{t12}^*, which can be clearly observed in Fig. 5 and Fig. 6. Each design graph of a unit-cell pattern is terminated such that $0 \leq H/L_{min} \leq 0.3$, where L_{min} denotes the length of the shortest struts of the unit-cell pattern. The values of H/L_{min} above 0.3 are not considered, to ensure that the Euler-Bernoulli beam theory is still reasonably applicable. It can be seen from Fig. 5 and Fig. 6 that the weight efficiency obtained from the body-centered square and the diamond-square unit-cell patterns is the same. The same is true for the triangular and kagome unit-cell patterns. In addition, it can be observed from Fig. 5 that, for bending, the square unit-cell pattern yields the best weight efficiency and the diamond unit-cell pattern yields the worst. In fact, the square and diamond patterns are the same pattern. The difference is only in the relative directions between the intended applied loads and the patterns. Although the square pattern yields the best weight efficiency for bending, the maximum effective bending rigidities that can be obtained from this unit-cell pattern without violating the limiting value of $H/L_{min} = 0.3$ is lower than that of the body-centered square pattern. From Fig. 6, for torsion, the diamond unit-cell pattern gives the best weight efficiency while the square unit-cell pattern gives the worst. Without violating the limit value of $H/L_{min} = 0.3$, the maximum torsional rigidity can be obtained from the body-centered square pattern.

Finally, to demonstrate how the closed-form effective properties presented in this study can be used in real applications, two 2D-lattice plates of hexagonal and triangular unit cells having rectangular struts with $B \times H = 6.40 \times 13.00$ mm are analyzed. The plates are clamped square plates of $\tilde{L} \times \tilde{L}$, where $\tilde{L} = 1{,}600$ mm, each with a point load $P = 1{,}000$ N applied at its center, as shown in Fig. 7(a). The characteristic length L of each plate's unit cells is selected such that the normalized area weight density ρ_A^*/ρ of the plate is equal to 2.2×10^{-3} mm. This yields the characteristic length $L = 43.67$ mm for hexagonal unit cells and $L = 131.01$ mm for triangular unit cells. The base material of the plates has Young's modulus $E = 200$ GPa and Poisson's ratio $\nu = 0.25$. As schematically shown in Fig. 7(b), an equivalent homogeneous plate with a thickness of $h = 13.00$ mm and a material having $E_i = E_i^*$, $\nu_{ij} = \nu_{ij}^*$, and $G_{12} = G_{12}^*$ is created for each 2D-lattice plate. The effective elastic properties, E_i^*, ν_{ij}^*, and G_{12}^*, are determined from the closed-form solutions in Table 2. The equivalent homogeneous plates are subjected to the same boundary conditions and load as the original ones. Subsequently, the deflections of the original lattices and their equivalent homogeneous plates, determined by finite element analysis, are compared. Fig. 8 shows the normalized deflections of the two 2D-lattice plates and their equivalent homogeneous plates along the X axis, defined in Fig. 7. Good agreement between the deflections of the 2D-lattice plates and of the equivalent homogeneous plates is observed. The differences between the load-point deflections of the original hexagonal and triangular lattices and their equivalent homogeneous plates are only 0.49% and 0.04%, respectively. These results demonstrate how the closed-form effective properties presented in this study can be used to predict the behavior of 2D-lattice plates in real applications. It can also be seen in Fig. 8 that the deflection of the hexagonal lattice is larger than that of the triangular lattice. It can be seen from Fig. 5 and Fig. 6 that the weight efficiency of triangular lattices is better than that of hexagonal lattices in both pure bending and torsion modes. Since both lattices have the same weight per area, it follows that the hexagonal lattice has smaller rigidities and, subsequently, larger deflection than the triangular lattice does as observed in Fig. 8.

7. Conclusions

In this study, the relationships between the effective rigidities and the area weight densities are used to determine the weight efficiency of 2D-lattice plates created from different unit-cell patterns. A method to design 2D-lattice plates, based on their weight efficiency, is proposed. The study considers 2D-lattice plates that consist of Euler-Bernoulli beams and can be modeled as homogeneous orthotropic Kirchhoff plates. The strain-energy-based homogenization method is used to determine these equivalent orthotropic Kirchhoff plates. In the homogenization method, a unit cell of the considered 2D-lattice plate is subjected to some curvature modes. The resulting analytical expressions of the strain energy are used to analytically compute the effective properties of the plates. The considered effective properties, presented as closed-form solutions, are the effective elastic constants, effective bending and torsional rigidities, and relationships between the effective rigidities and the area weight densities. The proposed design method employs the relationships between the effective rigidities and the area weight densities of 2D-lattice plates to determine their weight efficiency, and design solutions are determined from these relationships. Design formulas for different design inputs are derived. Examples of design graphs for 2D-lattice plates with different unit-cell patterns are presented and discussed. From the example cases, it is observed that, for bending, the square unit-cell pattern yields the best weight efficiency and the diamond unit-cell pattern yields the worst. For torsion, the diamond unit-cell pattern gives the best weight efficiency and the square unit-cell pattern gives the worst. In addition, the weight efficiency obtained from the body-centered square and the diamond-square unit-cell patterns is the same. The triangular and kagome unit-cell patterns also yield the same weight efficiency. Finally, the usefulness of the obtained weight efficiency is demonstrated through the analysis of 2D-lattice plates having different unit-cell patterns.

For future work, the present study can be extended to 2D-lattice plates that consist of Timoshenko beams and can be modeled accurately as frames of Timoshenko beams. This extension will allow closed-form design equations for 2D-lattice plates having thicker struts to be constructed. More significantly, the methodology of the present study can also be used to explore the weight efficiency of 3D lattices that are made up of beams. Closed-form design equations for 3D lattices may be constructed by considering their weight efficiency based on volume weight densities, instead of area weight densities. However, performing symbolic computation for 3D lattices may not be possible as the derivations can be too complex for any symbolic computational platform. In this case, the rigidities and weight density can be used to evaluate weight efficiency numerically instead.

Acknowledgements

Scholarships from the Center of Excellence in Material Science, Construction and Maintenance Technology and Sirindhorn International Institute of Technology, Thammasat University for the first author are greatly appreciated.

References

[1] V. V. Vasiliev, V. A. Barynin, and A. F. Rasin, "Anisogrid lattice structures—Survey of development and application," *Composite Structures*, vol. 54, no. 2–3, pp. 361-370, 2001.

[2] V. V. Vasiliev and A. F. Razin, "Anisogrid composite lattice structures for spacecraft and aircraft applications," *Composite Structures*, vol. 76, no. 1–2, pp. 182-189, 2006.

[3] G. Totaro and Z. Gürdal, "Optimal design of composite lattice shell structures for aerospace applications," *Aerospace Science and Technology*, vol. 13, no. 4, pp. 157-164, 2009.

[4] V. V. Vasiliev, V. A. Barynin, and A. F. Razin, "Anisogrid composite lattice structures—Development and aerospace applications," *Composite Structures*, vol. 94, no. 3, pp. 1117-1127, 2012.

[5] S. Gu, T. J. Lu, and A. G. Evans, "On the design of two-dimensional cellular metals for combined heat dissipation and structural load capacity," *International Journal of Heat and Mass Transfer*, vol. 44, no. 11, pp. 2163-2175, 2001.

[6] L. J. Gibson, "Biomechanics of cellular solids," *Journal of Biomechanics*, vol. 38, no. 3, pp. 377-399, 2005.

[7] I. Goda, M. Assidi, S. Belouettar, and J. Ganghoffer, "A micropolar anisotropic constitutive model of cancellous bone from discrete homogenization," *Journal of the Mechanical Behavior of Biomedical Materials*, vol. 16, pp. 87-108, 2012.

[8] G. Bertolino, M. Montemurro, and G. De Pasquale, "Multi-scale shape optimisation of lattice structures: An evolutionary-based approach," *International Journal on Interactive Design and Manufacturing (IJIDeM)*, vol. 13, no. 4, pp. 1565-1578, 2019.

[9] A. Catapano and M. Montemurro, "A multi-scale approach for the optimum design of sandwich plates with honeycomb core. Part I: homogenisation of core properties," *Composite Structures*, vol. 118, no., pp. 664-676, 2014.

[10] K. Theerakittayakorn, P. Suttakul, P. Sam, and P. Nanakorn, "Design of frame-like periodic solids for isotropic symmetry by member sizing," *Journal of Mechanics*, vol. 33, no. 1, pp. 41-54, 2017.

[11] Z.-X. Lu, X. Li, Z.-Y. Yang, and F. Xie, "Novel structure with negative Poisson's ratio and enhanced Young's modulus," *Composite Structures*, vol. 138, no., pp. 243-252, 2016.

[12] Z. Hashin, "Analysis of composite materials—a survey," *Journal of Applied Mechanics, Transactions ASME*, vol. 50, no. 3, pp. 481-505, 1983.

[13] D. Caillerie and J. C. Nedelec, "Thin elastic and periodic plates," *Mathematical Methods in the Applied Sciences*, vol. 6, no. 1, pp. 159-191, 1984.

[14] R. V. Kohn and M. Vogelius, "A new model for thin plates with rapidly varying thickness," *International Journal of Solids and Structures*, vol. 20, no. 4, pp. 333-350, 1984.

[15] P. M. Suquet, Elements of homogenization for inelastic solid mechanics, "Homogenization techniques for composite media," in *Lecture Notes in Physics*. Berlin: Springer-Verlag, 1987.

[16] S. J. Hollister and N. Kikuchi, "A comparison of homogenization and standard mechanics analyses for periodic porous composites," *Computational Mechanics*, vol. 10, no. 2, pp. 73-95, 1992.

[17] L. J. Gibson and M. F. Ashby, *Cellular Solids: Structure and Properties*, ed. Cambridge: Cambridge University Press, 1999.

[18] A. J. Wang and D. L. McDowell, "In-plane stiffness and yield strength of periodic metal honeycombs," *Journal of Engineering Materials and Technology, Transactions of the ASME*, vol. 126, no. 2, pp. 137-156, 2004.

[19] S. Gonella and M. Ruzzene, "Homogenization and equivalent in-plane properties of two-dimensional periodic lattices," *International Journal of Solids and Structures*, vol. 45, no. 10, pp. 2897-2915, 2008.

[20] A. Lebée and K. Sab, "A Bending-Gradient model for thick plates. Part I: Theory," *International Journal of Solids and Structures*, vol. 48, no. 20, pp. 2878-2888, 2011.

[21] A. Vigliotti and D. Pasini, "Linear multiscale analysis and finite element validation of stretching and bending dominated lattice materials," *Mechanics of Materials*, vol. 46, no. 0, pp. 57-68, 2012.

[22] F. Dos Reis and J. Ganghoffer, "Equivalent mechanical properties of auxetic lattices from discrete homogenization," *Computational Materials Science*, vol. 51, no. 1, pp. 314-321, 2012.

[23] A. Lebée and K. Sab, "Homogenization of a space frame as a thick plate: Application of the Bending-Gradient theory to a beam lattice," *Computers and Structures*, vol. 127, pp. 88-101, 2013.

[24] F. Dos Reis and J.-F. Ganghoffer, "Homogenized elastoplastic response of repetitive 2D lattice truss materials," *Computational Materials Science*, vol. 84, no., pp. 145-155, 2014.

[25] S. Malek and L. Gibson, "Effective elastic properties of periodic hexagonal honeycombs," *Mechanics of Materials*, vol. 91, no., pp. 226-240, 2015.

[26] K. Theerakittayakorn, P. Nanakorn, P. Sam, and P. Suttakul, "Exact forms of effective elastic properties of frame-like periodic cellular solids," *Archive of Applied Mechanics*, vol. 86, no. 8, pp. 1465-1482, 2016.

[27] P. Sam, P. Nanakorn, K. Theerakittayakorn, and P. Suttakul, "Closed-form effective elastic constants of

frame-like periodic cellular solids by a symbolic object-oriented finite element program," *International Journal of Mechanics and Materials in Design*, vol. 13, no. 3, pp. 363-383, 2017.
[28] R. Hill, "Elastic properties of reinforced solids: Some theoretical principles," *Journal of the Mechanics and Physics of Solids*, vol. 11, no. 5, pp. 357-372, 1963.
[29] J. Hohe, "A direct homogenisation approach for determination of the stiffness matrix for microheterogeneous plates with application to sandwich panels," *Composites Part B: Engineering*, vol. 34, no. 7, pp. 615-626, 2003.
[30] V. Alecci, S. B. Bati, and G. Ranocchiai, "Numerical homogenization techniques for the evaluation of mechanical behavior of a composite with SMA inclusions," *Journal of Mechanics of Materials and Structures*, vol. 4, no. 10, pp. 1675-1688, 2009.
[31] I. Masters and K. Evans, "Models for the elastic deformation of honeycombs," *Composite Structures*, vol. 35, no. 4, pp. 403-422, 1996.
[32] P. Suttakul, P. Nanakorn, and D. Vo, "Effective out-of-plane rigidities of 2D lattices with different unit cell topologies," *Archive of Applied Mechanics*, vol. 89, no. 9, pp. 1837-1860, 2019.
[33] D. W. Abueidda, M. Elhebeary, C.-S. A. Shiang, S. Pang, R. K. A. Al-Rub, and I. M. Jasiuk, "Mechanical properties of 3D printed polymeric Gyroid cellular structures: Experimental and finite element study," *Materials & Design*, vol. 165, no., pp. 107597, 2019.
[34] F. Auricchio, A. Bacigalupo, L. Gambarotta, M. Lepidi, S. Morganti, and F. Vadala, "A novel layered topology of auxetic materials based on the tetrachiral honeycomb microstructure," *Materials & Design*, vol. 179, no., pp. 107883, 2019.
[35] L. Yang, R. Mertens, M. Ferrucci, C. Yan, Y. Shi, and S. Yang, "Continuous graded Gyroid cellular structures fabricated by selective laser melting: Design, manufacturing and mechanical properties," *Materials & Design*, vol. 162, no., pp. 394-404, 2019.
[36] A. Catapano and M. Montemurro, "A multi-scale approach for the optimum design of sandwich plates with honeycomb core. Part II: The optimisation strategy," *Composite Structures*, vol. 118, no., pp. 677-690, 2014.
[37] M. Montemurro, A. Catapano, and D. Doroszewski, "A multi-scale approach for the simultaneous shape and material optimisation of sandwich panels with cellular core," *Composites Part B: Engineering*, vol. 91, no., pp. 458-472, 2016.
[38] M. Montemurro, G. Bertolino, and T. Roiné, "A general multi-scale topology optimisation method for lightweight lattice structures obtained through additive manufacturing technology," *Composite Structures*, vol. 258, no., pp. 113360, 2021.
[39] T. Baran and M. Öztürk, "In-plane elasticity of a strengthened re-entrant honeycomb cell," *European Journal of Mechanics-A/Solids*, vol. 83, no., pp. 104037, 2020.
[40] S. Timoshenko and J. N. Goodier, in *Theory of Elasticity*, ed. New York: McGraw-Hill book Company, 1951.

Pana Suttakul, photograph and biography not available at the time of publication.

Ekachai Chaichanasiri, photograph and biography not available at the time of publication.

Pruettha Nanakorn, photograph and biography not available at the time of publication.